Improvement of the optical and photocatalytic properties of ZnAl2O4: 1% La3+, x% Pb2+ nanoparticles synthesized by citrate sol-gel route

Hichem Filali (hichemfilali5@yahoo.com)
Universite Freres Mentouri Constantine 1 faculté des sciences exactes
Nahman Boukheit
Laboratoire de Thermodynamique et Traitements de Surface des Matériaux, Université Frères Mentouri, Constantine 1, Algérie
Rafika Bouhroum
Laboratoire des Techniques Innovantes et Préservation de l'Environnement, Université Frères Mentouri Constantine 1, Algérie
Wassila Chekirou
Laboratoire de Thermodynamique et Traitements de Surface des Matériaux, Université Frères Mentouri, Constantine 1, Algérie
Ahcène Karaali
Laboratoire de Thermodynamique et Traitements de Surface des Matériaux, Université Frères Mentouri, Constantine 1, Algérie

Research Article

Keywords: ZnAl2O4, nanoparticles, Sol-gel, doping, photocatalytic

Posted Date: March 18th, 2021

DOI: https://doi.org/10.21203/rs.3.rs-316386/v1

Improvement of the optical and photocatalytic properties of $ZnAl_2O_4$: 1% La^{3+}, x% Pb^{2+} nanoparticles synthesized by citrate sol-gel route

H. Filali [a*], N. Boukheit [a], R. Bouhroum [b], W. Chekirou [a], A. Karaali [a].

[a] *Laboratoire de Thermodynamique et Traitements de Surface des Matériaux, Université Frères Mentouri, Constantine 1, Algérie.*

[b] *Laboratoire des Techniques Innovantes et Préservation de l'Environnement, Université Frères Mentouri Constantine 1, Algérie.*

[*] hichemfilali5@yahoo.com

Improvement of the optical and photocatalytic properties of $ZnAl_2O_4$: 1% La^{3+}, x% Pb^{2+} nanoparticles synthesized by citrate sol-gel route

Abstract

Samples of pure zinc aluminate ($ZnAl_2O_4$) and doped both with lead (Pb^{2+}) at different ratios (0, 0.5, 1, 1.5, 2 and 2.5% mol) and a constant amount of lanthanum (La: 1% mol), were prepared by the citrate sol-gel technique, and then annealed at 900°C for 2h. In order to study the structural, optical and thermal properties; different characterization methods were used, such as: powder X-ray diffraction (XRD), scanning electron microscope (SEM), energy dispersive X-ray spectroscopy (EDX), differential scanning calorimetry (DSC), TGA, Fourier transform infrared spectroscopy (FTIR) and Raman spectroscopy. The Analyzes by XRD revealed the presence of the cubic single phase $ZnAl_2O_4$ for all samples, with a crystallites size between 19 and 25 nm. These results were confirmed using FTIR, Raman spectroscopy and SEM. Also, photocatalytic study for different samples of $ZnAl_2O_4$ shows that they can be used like as photocatalyst and good adsorbents for degradation of Hexamethyl crystallized violet dye in aqueous solution.

Keywords: word; $ZnAl_2O_4$, nanoparticles, Sol-gel, doping, photocatalytic.

1. Introduction

Spinel $ZnAl_2O_4$, has a high thermal and chemical stability, a high mechanical strength and a low surface acidity [1, 2], its wide band gap energy (Eg~3.8 eV) [1, 3-7], its particle size, and large surface area, make it a material of choice for a variety of applications, such as heterogeneous catalysis and adsorption of molecules [8]. Also, zinc aluminate has been recently considered as a functional material in host luminescent applications [9]. Moreover, $ZnAl_2O_4$ has been widely employed as a good host phosphor material as a result of uniform particle and narrow size distribution [10]. For effective doping, rare earths or lanthanides are widely used as activators in luminescent materials due to high emission properties [4-7, 11- 12]

On the other hand, adsorption is a technique that consists of fixing the pollutants on the surface of an adsorbent without altering the pollutant. It is very widely used as a refining treatment. Photocatalyst is also aims to eliminate organic micro pollution, but unlike adsorption, its ultimate goal is to degrade or even mineralize organic pollutants.

In recent years, zinc aluminate has been largely used as a photocatalyst for degradation of organic pollutants in water such as dyes. In our work also tested it as an adsorbent to remove the HCV dye. The crystal violet dye was considered as a low biodegradable and

very persistent organic pollutant. Its presence in aquatic environments can be detrimental to animal and plant species as well as to the various microorganisms living in these waters. The absorption of the HCVs is maximal at the wavelength 590 nm. Therefore, in order to assess the effectiveness of the synthesized $ZnAl_2O_4$ powder and even what field it can be used in; the water treatment area was tested as a photocatalysts to purify the water from organic pollutants [9].

It is known that, zinc aluminate has the normal spinel structure and the chemical formula of AB_2O_4 in which Zn^{2+} (A) ions occupy tetrahedral sites and Al^{3+} (B) ions the octahedral sites. In general, A and B cations can reside on both T and M sites, thus giving rise to a variable disorder degree, which can be described using the inversion parameter i, defined as the fraction of the B cations at the T sites. The inversion parameter can therefore vary from 0, in the completely normal spinel $^{T}A^{M}B_2O_4$, to 1, in the completely inverse spinels $^{T}B\ ^{M}(AB)\ O_4$; while the value 2/3 is assuming for a completely random (i.e. disordered) cation distribution [17]. Many synthesis methods preparation of $ZnAl_2O_4$ have been reported, such as: hydrothermal [10, 18]; citrate [1, 19, 20], sol-gel [21-22], combustion [13, 23- 25], pyrolysis [14, 26], co-precipitation [15, 27- 29] and solvothermal [30-31]. While doping $ZnAl_2O_4$ was carried out with transition metals or rare earths depending on the intended application [6-7, 14, 32].

In this present study, we have used the citrate sol-gel method for preparing samples of pure $ZnAl_2O_4$ and dual doped by a constant concentration of La^{3+} (1% mol) and x% mol Pb^{2+} with_different amounts of Lead (0, 0.5, 1, 1.5, 2, and 2.5% mol).The materials annealed at 900°C for 2h have been characterized for their structural and optical properties. In addition, we have prepared a sample $ZnAl_2O_4$ containing 50% by weight of ZnO in order to better characterize the effectiveness of the two purification methods, notably photocatalysis and adsorption.

2. Methods and Materials

2.1 Synthesis of $ZnAl_2O_4$

To prepare the $ZnAl_2O_4$ powder, 2.19 g of Zinc Acetate dihydrate ($C_4H_6O_4Zn.2H_2O$) was mixed with 20 ml of distillated water and stirred magnetically for 30 minutes. On the other hand, another solution contains 7.5 g of Aluminum nitrate nonahydrate ($Al(NO_3).9H_2O$) and 20 ml of distillated water was prepared with the same preceding method. The two solutions were mixed well using the citric acid ($C_6H_8O_7$) as chelating

agent. Then the resulted mixture was dried on hot plate at 80°C during 90 minutes. The doped $ZnAl_2O_4$ solutions were prepared exactly like the pure one. A constant amount of Lanthanum Acetate hydrate ($La(CH_3CO_2)_3.H_2O$) (1 % mol) was added in the first solution of Zinc. On the other hand, different amount of Lead (II) Acetate trihydrate ($C_4H_6O_4Pb.3H_2O$) was added to the second solution of Aluminum nitrate (0, 0.5,1, 1.5, 2 and 2.5 % mol). After drying the mixture obtained, it is subjected to a heat treatment at 900°C for 2h in an oven. Finally, we have seven samples called pure $ZnAl_2O_4$, S0, S1, S2, S3, S4 and S5 respectively.

2.2 Photocatalytic and adsorption

To test the reactivity of the two processes on the HCV molecules, a solution containing HCV with concentrations equal to 5 mg/l and 0.1g for each sample of $ZnAl_2O_4$ powder has prepared. The evolution of HCV was followed as a function of time of contact, by the measurement of the absorption at 590 nm. In photocatalytic activity, a cylindrical Pyrex photo reactor initiated by UV mercury lamp (350 W) placed in center of a closed enclosure, the solution of HCV and the catalyst were stirred in the dark for 30 minutes to establish the adsorption-desorption equilibrium. After each appropriate time interval, 5 ml aliquots was sampled and filtered using 0, 22 µm membranes filters (S-PAK), to remove the solid phase thus allowing the analyze by spectrophotometer (SHIMADZU, UV-1800).

2.3 Characterization

The obtained powder was characterized by X-ray diffraction using $Cu_{K\alpha}$ radiation Bruker (D8 Advance) X-ray diffractometer. The structural composition of powders was studied using m-Raman spectrometer (Jobin-Yvon). Optical properties were analyzed using UV–visible spectrophotometer (Shimadzu, UV-1800). The Morphological studies of powders were carried out by Scanning Electron Microscopy (Philips XL30 S-FEG). FT-IR analysis was carried away using KBr disc technique on a FT-IR spectrometer Bruker IFS66v. EDX measurements have been performed with a Hitachi S-3000N scanning electron microscope and the thermal analysis of dried gel was studied by STA 449 F3 Jupiter®.

3. Results and discussions

3.1. Powder X-ray diffraction

Figure 1.a shows the XRD diagrams of pure $ZnAl_2O_4$ and samples S0, S1, S2, S3, S4 and S5. All patterns show the characteristic diffraction peaks corresponding to (111), (220), (311), (400), (331), (422), (511), (440),(620),(533),(642),(731) reflections of cubic $ZnAl_2O_4$ spinel structure (JCPDS No. 05-0669). These results show the existence of traces impurities such as ZnO on some samples. The degree of crystallinity is calculated from the XRD spectra of the samples:

$$C\,(\%) = \frac{\text{Area of crystalline peaks} * 100}{\text{Area of all peaks}}$$

, and the results are presented in Table 1.The average size of the crystallites (D) was calculated from the five most intense X-ray diffraction peaks, using Scherrer's formula (1), [7, 16-18].

$$D = \frac{0.9\lambda}{\beta \cos\theta} \qquad (1)$$

Where λ is the wavelength of Cu-Kα (0.15406 nm), β is the full width at half maximum (FWHM) of the peak and θ is the Bragg angle. We found average crystallites size between 19 and 25 nm for S2 and S5, respectively (Table 1). In addition, we noticed a slight shift of the peaks of the S0 sample towards the low angles compared to the pure sample of $ZnAl_2O_4$. This suggested that the increase in lattice parameter is most likely due to the presence of La^{3+} in $ZnAl_2O_4$ system. Because, the ionic radius of La^{3+} (1.04 Å) [27] is greater than those of the tetrahedral (Zn^{2+} (0.60 Å), Al^{3+} (0.39 Å)) and octahedral (Zn^{2+} (0.74 Å, Al^{3+} (0.54 Å)) sites of $ZnAl_2O_4$ system [19]. Similar results have been previous observed in the $ZnAl_2O_4$ doped by Lanthanides elements [11, 14, 18].The most intense (220) and (311) diffraction peaks for all samples are illustrated in figure 1.b. We observe also that when Pb^{2+} is added up to 1.5 % mol to the S0 sample, the shift of the most intense peaks is towards the large angles, then beyond this percentage of Pb^{2+}, the shift changes by meaning. Although the ionic radius of Pb^{2+} (1.23 Å) [32] is greater than those of Zn^{2+} and Al^{3+}, the Vegard's law is violated up to 1.5% mol. The lattice parameters (a) for all samples are presented in Table 1. The variation of the lattice parameter of the samples versus of the % Pb^{2+} is represented by figure 1.c, and shows well the parabolic behavior relationship to Pb^{2+}mol %. This result

can be explained by the decrease in the electronic cloud of the outer layer of Pb^{2+}, due to its electronic interactions with a greater number of closer neighbors Zn^{2+}, which makes it smaller than the Zn^{2+} ion. As the percentage of Pb^{2+} is increased, the shrinkage must be smaller; therefore, the lattice parameter should be increase. We note a similar phenomenon was observed by S.V. Motlung and al. [33].

3.2 FTIR spectroscopy

The fig. 2 represents the IR spectra of the samples pure $ZnAl_2O_4$ and S0, S1, S2, S3, S4 and S5. We observe the same absorption bands in all spectra, such the broad band centered on 3400 cm^{-1} and the band 1615 cm^{-1}.These are related to the OH stretching vibration and H_2O deformation vibration, respectively. Also, the presence of three absorption bands located at 643, (550-565) and 501 cm^{-1} comes from the stretching and bending modes vibration of octahedral bonds (AlO_6)[34-36]. These bands are characteristic of the $ZnAl_2O_4$ spinel structure. The sharp absorption band at 2300 cm^{-1} is due to the stretching vibration mode of CO_2. The adsorption of water and carbon dioxide from the atmosphere may be due to the very high specific surface area of these materials [37]. No other impurity phase is detected by FTIR spectra, and is in good agreement with the results obtained by XRD.

3.3 DSC and TGA

The behavior of the gel as a function of temperature was studied by continuous heating using simultaneously thermo gravimetric analysis (TGA) and differential scanning calorimetry (DSC). The thermal cycle applied under an atmosphere of neutral nitrogen consists of heating from ambient temperature to 1000 °C at a speed of 10 °C / min, followed by holding at this temperature for 10 minutes, and cooling to ambient temperature. The TGA and DSC pattern of pure $ZnAl_2O_4$ is record and depicted in fig.3. The TGA and DSC curves of all samples are almost similar. Thermo gravimetric analysis reveals that the thermal decomposition of precursors takes place in four stages (see fig.3.a): The first loss of mass (~14 %) is observed between room temperature and 210 °C. It probably corresponds to the dehydration of the gel (adsorbed water). A second mass loss (9 %), starts at 210 °C and ends at 310°C [38]. It can only be attributed to the decomposition of nitrates. The third stage reveals a significant loss of mass (~ 37 %) which is mainly due to the combustion of acetates and citric acid.

Finally, a weak mass loss (~ 8%) which begins at 550 °C and ends in the vicinity of 1000 °C. This mass loss probably corresponds to the removal of the hydroxyl groups. The total weight loss is approximately 68% of the initial mass of the precursor at 1000°C.

On DSC curves during heating, phase changes cause absorption or release of heat, which manifests as an endothermic (exothermic) peak during the reaction. The DSC analysis curve (fig.3.b) shows the existence of several peaks:

- A large peak at 110 °C corresponding to the evaporation of water
- Two exothermic peaks at 417 and 655 °C, the first can be attributed to the formation of aluminum and zinc hydroxide phases, and the second broad peak is due to the formation of the cubic structure spinel $ZnAl_2O_4$. We have also noticed that the increase in the quantities of Pb leads to the small displacement of the peaks towards the low temperatures.

3.4 Raman analysis

It is well known that Raman spectroscopy is a characterization method to measure the frequencies of the long-wavelength lattice vibrations (phonons). Raman spectroscopy provides a fast and convenient method for detecting small structural changes in materials. On the other hand, according to group theory, $ZnAl_2O_4$ should exhibit five Raman active modes: $A_{1g}+ E_g+3T_{2g}$ [38]. However, the figure 4 displays Raman spectra of all samples treated at 900°C for 2h. These spectra are similar and reveal the presence of four peaks located at 196, 419,512 and 660 cm^{-1} and correspond, respectively, to T_{2g}, E_g ,T_{2g}, , and T_{2g} phonon frequencies of $ZnAl_2O_4$ spinel structure [20,38-40]. In addition, peak T_{2g} (3) at 660 cm^{-1} is most intense and represents the fingerprint of $ZnAl_2O_4$ spinel [17]. Obviously, the peak located at 727 cm^{-1} corresponding to the active mode A_{1g} is not observed on our spectra. This peak is attributed to the symmetrical stretching vibration Al-O of the AlO_4 groups created by the redistribution of certain aluminium ions from the octahedral sites to the tetrahedral sites [41]. Therefore, the $ZnAl_2O_4$ spinel formed in our samples shows very little inversion. Furthermore, the E_g peak at 419 cm^{-1}also does not show the asymmetry typical of disordered $ZnAl_2O_4$ spinel as shown in figure 5 [38]. We can conclude that the results obtained by Raman spectroscopy confirm those found by X-ray diffraction.

3.5 UV-VIS

The diffuse reflectance spectra of the samples annealed at 900 °C for 2h in a range of 240 to 800 nm are presented in figure 6. For all the samples, we observed an absorption band in the UV (220-270 nm) region, which can be attributed to the band-to-band transition of the AlO6 in $ZnAl_2O_4$ spinel [42-43]. Another absorption band appears at 460 nm for the S0 sample and which shifts towards low wavelengths up to 1% mol Pb^{2+}, then it takes the reverse path up to 350 nm (S4 sample), to finally disappear giving a wide band for sample S5. This band arises from the defects absorption within the spinel material. Also, we notice that the absorption edge shifts slightly towards the low energies, with increase of % Pb^{2+} doping. However, in the VIS region from 450 to 720 nm, the reflectance improves with the increase of the doping (% mol Pb^{2+}). The maximum reflectance is obtained for 1% mol La^{3+} and 0% Pb^{2+} (S0 sample). We note, that this improvement of reflectance has been observed also in Sm (0.5% mol): $ZnAl_2O_4$ nanomaterials synthesized by vibrational milling [11].

The band gap energy (Eg) of the $ZnAl_2O_4$ samples can be determined from plots of $(K.h\nu)^n$ versus hν shown in figure 7 (with n = 2, which is appropriate for a direct band gap material such as $ZnAl_2O_4$) using the Tauc relation given in Equation (4)

$$(K.h\nu)^2 = C\,(h\nu - Eg) \qquad (4)$$

Where K is the Kubelka-Munk function [35] given in equation (5):

$$K = (1-R)^2/(2R) = F(R) \qquad (5)$$

R is reflectance (%), hν is the photon energy, C is a proportionality constant, and Eg band gap energy. The determination the intercept on the hν axis by extrapolating the linear part of the plot to $(K \times h\nu)^2 = 0$ as shown in figure 7, give the band gap energy (E_G). The values of the obtained optical band gaps are: 3.95; 3.85; 3.70; 3.60; 3.48; 3.34 and 3.05 eV for pure $ZnAl_2O_4$, S0, S1, S2, S3, S4 and S5 samples respectively. These results confirm the displacement of the absorption edge towards large wavelengths with the increase of the % Pb as well as the change of the forbidden band of $ZnAl_2O_4$ doped with Pb^{2+}.

3.6 Scanning electron microscopy

The observations of this micrograph allow us to say that the morphology of the grains is irregular (fig.8). It varies from a spheroid shape for small particles to an elongated shape for large particles. The particle size is widely distributed with an average size of around 100 nm. This leads to the conclusion that the crystallites tend to agglomerate in small clusters [44], giving nanoparticles having sizes much larger than those of the crystallites (25 nm) calculated from Sherrer's formula.

3.7 EDX

Figure 9, showing the spectrum of pure $ZnAl_2O_4$, clearly indicates the detection of the elements (Zn, Al, and O) present in pure zinc titanate. While in fig. 9.b, which represents the spectrum of sample S1, we note, in addition to the matrix elements, the presence of dual doping elements (La and Pb) [45]. We also observe on the other spectra which are not represented here, that the intensity of the lead peak increases when the percentage of the latter increases. The presence of carbon comes from the metallization of the samples.

3.8 Photocatalytic activity

As shown in Fig. 10, the degradation of HCV by direct photolysis requires which may appear in practice too long; this renders the process of little benefit to environmental applications as compared to other methods. For this reason, we examined: (i) adsorption and (ii) photo catalysis. Experimentally, the only difference between the two processes is the absence and presence of ultraviolet radiation in adsorption and photocatalysts respectively.

Figure 11 (a), (b) and (c) compares the results obtained with those of direct photolysis, it is clear that the addition of $ZnAl_2O_4$ powder of different types in the reaction medium considerably accelerates the degradation of the dye. Besides to that the dispersion rate is different compared to the powder used.

Before UV-light irradiation, each suspension of photocatalysts/HCV solutions was continuously stirred in the dark for 30 min to reach an adsorption-desorption equilibrium. For the entire sample, the adsorption efficiency of HCV varied between 0 and 30%, 45% and 55% in $ZnAl_2O_4$-ZnO, pure $ZnAl_2O_4$ and S5 respectively. These

results indicate that the synthesized $ZnAl_2O_4$ is good adsorbent, what encouraged us to continue the study of adsorption.

After 120 min of irradiation, the dye degrades by 75%, 70% and 57% by ($ZnAl_2O_4$ + ZnO), S5 and pure $ZnAl_2O_4$, respectively. The difference in dye removal rate depends on the body used. Pure $ZnAl_2O_4$ is the least efficient catalyst. However, the presence of Pb and ZnO respectively, in the other two samples S5 and ($ZnAl_2O_4$ + ZnO), makes them more potent.

This is due to the fact that the atoms of lead replace the atoms of Zn and Al, which creates surface exchanges and an increase in the lattice parameter as well as a decrease in gap energy (~ 3 eV) , making sample S5 more powerful and efficient than pure $ZnAl_2O_4$ (Eg = 3.9 eV). As for ($ZnAl_2O_4$ + ZnO), it is the most efficient because of its structure, its wide band gap (3 eV) and its excitonic energy of 60 meV; the highest value of all semiconductors [46]. In this study, we observe that the photocatalytic behavior of zinc aluminates strongly depends on the energy of the forbidden band (Eg) [47].

3.8.1 Discussion photocatalytic Activity

The photon excitation of $ZnAl_2O_4$ amounts to creating electron-hole pairs, that is, a redox system, by passing the electrons (e^-) from the valence band (BV) to the conduction band (BC) creating a positive hole (h^+) in BV.

The created holes move to the surface of the material where their high oxidizing power manifests itself towards the adsorbed oxidizable species. While the electrons produced act on the reducible adsorbed species. It is accepted that in an aerated environment, the electrons, which have acquired the energy of the conduction band, are captured by the adsorbed oxygen to give superoxide radical ions and a new state of equilibrium being established on the oxide surface [48- 50]. In our case, the electron donors can be H_2O, OH^- or the pollutant HCV.

The mechanism of photo catalysis includes the following reactions:

$$ZnAl_2O_4\ (ZnO) + h\nu \rightarrow ZnAl_2O_4\ (ZnO) + h+ + e^-$$

$$H_2O + h^+ \rightarrow \cdot OH + H+$$

$$OH^- + h^+ \rightarrow \cdot OH$$

$$O_2 + e- \rightarrow O_2^{\cdot -}$$

$$HCV\ (P) + \cdot OH\ (O_2^{\cdot -}) \rightarrow H_2O + CO_2$$

3.9 Adsorption Activity

When the three solutions are stirred in the dark for 30 minutes, the three samples studied prefer adsorption to photo-catalysis. Figure 11. (d) indicates the monitoring of adsorption as a function of contact time (under the same conditions as photocatalysis (temperature, concentration, etc.)), allows to conclude on the one hand that the adsorption is remarkable for three samples and on the other hand that the retention rate is 50, 42 and 25% on S5, pure $ZnAl_2O_4$ and $ZnAl_2O_4$ + ZnO after 30 minutes, respectively.

After 150 minutes of contact, the remaining amount of HCV decreases and the adsorbed amount increases, the dispersion rate was found to be 64%, 60% and 50% in the presence of $ZnAl_2O_4$+ZnO, S5 and pure $ZnAl_2O_4$ respectively.

In the case of pure and doped $ZnAl_2O_4$, the curves have two important parts, between [0.30mn] the curve is linear, there is a rapid degradation with a high speed and more important for S5. After 30 minutes of contact, the degradation decreases with a slow and constant speed, and the curves have a flat level.

This is explained by the rapid fixation of the molecules in the first moments, because in addition to the presence of surface pores, there is a great affinity between the molecules of the dye and of the adsorbent. The formation of the kinetic plateau (C / C0) informs us that all the pores are occupied by molecules of HCV.

Concerning the $ZnAl_2O_4$ + ZnO sample, the adsorption is slow because from the first moments of contact up to 150 minutes, the HCV molecules slowly bind to the surface because there is a lack of affinity between ZnO and HCV molecules. On the other hand, the same isothermal model of Langmuir confirms this adsorption.

We found that the binding rate of HCV molecules is higher for the samples of S5 and pure $ZnAl_2O_4$ than for the sample $ZnAl_2O_4$ + ZnO. The affinity between the adsorbate and the adsorbent and the adsorbents structures strongly influence the binding performance, i.e. the speed fixation of the HCV molecules. in addition, doping with divalent or trivalent ions at the aluminum site can modify the structure of spinel aluminates [51]. Polarization in spinel aluminates is determined by the trivalent aluminum ion at the octahedral site [52 - 55].

4. Conclusion

The $ZnAl_2O_4$: 1% La^{3+}, x% Pb^{2+} powders was successfully prepared by citrate sol-gel technique. The Raman and DRX results confirmed that all samples prepared are consisted of single-phase cubic spinel structure without other impurity phases; in addition the formation of spinel that verified through TGA/DTA analysis. Moreover, the FTIR results confirmed the presence of absorption bands from stretching and bending vibration modes of octahedral bonds (AlO6) which correspond to a formation of normal $ZnAl_2O_4$. Meanwhile, the average value of crystallite size decrease with the increase of Pb^{2+} doping up to 1% mol (19nm), and then it increases to reach 25nm at 2.5% mol Pb^{2+}. Regarding the lattice parameter, we notice that the Vegard's law is violated up to 1.5% mol Pb^{2+}, i.e. the lattice parameter decreases instead of increasing. On the other hand, UV-Visible spectra indicate that the band gap of the dual doped samples decreased with the increase of Pb^{2+} content ion concentration. Meanwhile, reflectance spectra revealed that absorption edge of $ZnAl_2O_4$ powders had shifted to lower energy by the addition of Pb^{2+} content. From the previous results, the presence of the elementary composition for all samples was confirmed through the EDX analysis. Finally, photocatalytic study for different samples of $ZnAl_2O_4$ shows that they can be used like as photocatalysts and good adsorbents for degradation of Hexamethyl crystallized violet dye in aqueous solution.

Acknowledgements

We, the authors, thank the Autonoma University Spanish Laboratory, especially doctor M.Mansosilvan, for providing all the facilities required to conduct experiments in very good conditions.

References:

[1] Battiston S, Rigo C, E. Severo da C, et al. Synthesis of zinc aluminate ($ZnAl_2O_4$) spinel and its application as photocatalyst. Materials Research. 2014; 17(3):734–738.

[2] Wang S.-F, Sun G.-Z, Fang L.-M, et al. A comparative study of $ZnAl_2O_4$ nanoparticles synthesized from different aluminum salts for use as fluorescence materials, Scientific Reports. 2015; 5(12849).

[3] Shahmirzaee M, Shafiee Afarani M, Arabi AM, et al. In situ crystallization of $ZnAl_2O_4$/ZnO nanocomposite on alumina granule for photocatalytic purification of wastewater. Res Chem Intermed. 2016; 43:321–340.

[4] Li X, Zhu Z, Zhao Q, et al. Photocatalytic degradation of gaseous toluene over $ZnAl_2O_4$ prepared by different methods: A comparative study. Journal of Hazardous Materials. 2011; 186(2-3):2089–2096.

[5] Zhang L, Yan J, Zhou M, et al. Fabrication and photocatalytic properties of spheres-in-spheres ZnO/$ZnAl_2O_4$ composite hollow microspheres, Applied Surface Science 2013; 268:237–245.

[6] Buvaneswari K, Vetha G, Andal V. Green synthesis of $ZnAl_2O_4$ nanoparticles for the degradation of methyl orange dye under visible light. ChemTech. 2015; 8(5):06-09.

[7] Ianoş R, Borcănescu S, Lazău R. Large surface area $ZnAl_2O_4$ powders prepared by a modified combustion technique. Chemical Engineering Journal. 2014; 240:260-263.

[8] Zhao L, Li XY, Zhao J. Fabrication, Characterization and Photocatalytic Capability of $ZnAl_2O_4$ Nanospheres, Advanced Materials Research, 2012; 518-523:736–739.

[9] Song X, Zheng S, Zhang J, et al. Synthesis of monodispersed $ZnAl_2O_4$ nanoparticles and their tribology properties as lubricant additives. Materials Research Bulletin. 2012; 47:4305–4310.

[10] Tsai M-T, Chang Y-S, Huang I-B, et al. Luminescent and structural properties of manganese-doped zinc aluminate spinel nanocrystals. Ceramics International. 2013; 39:3691–3697.

[11] Mekprasarta W, Boonyarattanakalina K. Pecharapaa W, et al. Optical characteristics of samarium doped $ZnAl_2O_4$ nanomaterials synthesized by vibrational milling process. Materials Today: Proceedings. 2018; 5:14126–14130.

[12] Dutta DP, Ghildiyal R, Tyagi AK. Luminescent Properties of Doped Zinc Aluminate and Zinc Gallate White Light Emitting Nanophosphors Prepared via Sonochemical Method. Journal of Physical Chemistry C**.** 2009;113:16954–16961.

[13] Peng C, Guo J, Liu M, et al. Enhanced ethanol sensing properties based on Sm_2O_3-doped ZnO, Nanocomposite. RSC Advances. 2014; 4:64093–64098.

[14] Kumar M, Natarajan V, Godbole SV, Synthesis, characterization, photoluminescence and thermally stimulated luminescence investigations of orange red-emitting Sm^{3+}-doped $ZnAl_2O_4$ phosphor. Bull. Mater. Sci. 2014; 37:1205–1214.

[15] Mahajan R, Kumar S, Prakash R, ety al. Synthesis and luminescent properties of Sm^{3+} doped zinc aluminate phosphor. AIP Conference Proceedings. 2018; 1953:1-4.

[16] Prakash R, Kumar S, Mahajan R, et al. Spectral properties of Dy^{3+} doped $ZnAl_2O_4$ phosphor, AIP Conference Proceedings. 2018; 1953:1-4.

[17] D'Ippolito V, Andreozzi GB, Bersani D, et al. Raman fingerprint of chromate, aluminate and ferrite spinels. J. Raman Spectrosc. 2015; 46:1255–1264.

[18] Dwibedi D, Murugesan C, Leskes M, et al. Role of annealing temperature on cation ordering in hydrothermally prepared zinc aluminate ($ZnAl_2O_4$) spinel. Materials Research Bulletin. 2018; 98:219-224.

[19] Elakkiya V**,** Sumathi S, Ce and Fe doped gahnite: Cost effective solar reflective pigment for cool coating applications, Journal of Alloys and Compounds. 2020; 820:153174.

[20] Motloung SV, Tshabalala KG, Kroon RE, et al. Effect of Tb^{3+}concentration on the structure and optical properties of triply doped $ZnAl_2O_4$:1% Ce^{3+},1% Eu^{3+}, x% Tb^{3+}nano-phosphors synthesized via citrate sol-gel method. Journal of

Molecular Structure. 2019; 1175:241-252.

[21] Tangcharoen T, T-Thienprasert J, Kongmark C, Effect of calcination temperature on structural and optical properties of MAl_2O_4 (M = Ni, Cu, Zn) aluminate spinel nanoparticles. Journal of Advanced Ceramics. 2019;8 :352–366.

[22] Zhou AP, Zhang D, Gong ZQ, et al. The structure and photoluminescence performances of $Zn_xAl_2O_4:Cr^{3+}$crystals with various annealing temperatures. Optoelectronics and Advanced Materials – Rapid Communications. 2018; 12:588-594.

[23] Singh V, Singh N, Pathak MSet al. Singh, Annealing effects on the luminescence properties of Ce doped $ZnAl_2O_4$ produced by combustion synthesis. Optik. 2018; 155:285-291.

[24] Mirbagheri SA, Masoudpanah SM, Alamolhoda S. Structural and optical properties of $ZnAl_2O_4$ powders synthesized by solution combustion method: Effects of mixture of fuels. Optik. 2020; 204:164170.

[25] Priya R, Negi A, S. Singla, et al. Luminescent studies of Eu doped $ZnAl_2O_4$ spinels synthesized by low-temperature combustion route. Optik. 2020; 204:164173.

[26] Chenga Y, Suna K, Ge P, Up-conversion luminescence in Yb^{3+}/Er^{3+} co-doped $ZnGa_2O_4$ and $ZnAl_2O_4$ powder phosphors. Optik. 2018; 170:1–9.

[27] Liu J, Zhou W, Jiang D, et al. Insights into the Doping Effect of Rare-Earth Metal on $ZnAl_2O_4$ Supported PtSn Catalyzed Isobutane Dehydrogenation. Catalysis Today. 2020 doi:10.1016/j.cattod.2020.04.016.

[28] Akika FZ, Benamira M, Lahmar H, et al. Structural and optical properties of Cu-doped $ZnAl_2O_4$ and its application as photocatalyst for Cr(VI) reduction under sunlight. Surfaces and Interfaces. 2020;18:100406.

[29] Somraksa W, Suwanboon S, Amornpitoksuk P, et al. Physical and Photocatalytic Properties of $CeO_2/ZnO/ZnAl_2O_4$ Ternary Nanocomposite Prepared by Co-precipitation Method, Mat. Res. 2020; 23(1):e20190627.

[30] Zhang D, Qiu YH, Xie YR, et al. The improvement of structure and photoluminescence properties of $ZnAl_2O_4:Cr^{3+}$ ceramics synthesized by using

solvothermal method. Materials and Design. 2017; 115:37–45.

[31] Femila Komahal F, Nagabhushana H, Basavaraj RB, G.P. et al. Solvothermal synthesis and luminescent properties of hierarchical flowerlike $ZnAl_2O_4:Ho^{3+}$ microstructures. Optical Materials. 2018; 84:536–544.

[32] Singh V, Tiwari MK. UV emitting Pb^{2+} doped $Ca_2La_8(SiO4)_6O_2$ phosphors prepared by sol-gel procedure. Optik. 2020; 206:163600.

[33] Motloung SV, Dejene FB, Swart HC.et al. Effects of Pb2+ions concentration on the structure and PL intensity of Pb-doped $ZnAl_2O_4$ nanocrystals synthesized using sol–gel process. Journal of Sol-Gel Science and Technology. 2014; 70:422–427.

[34] Elakkiya V, Sumathi S, Ce and Fe doped gahnite: Cost effective solar reflective pigment for cool coating applications. Journal of Alloys and Compounds. 2020; 820:153174.

[35] Staszak W, Zawadzki M, Okal J. Solvothermal synthesis and characterization of nanosized zinc aluminate spinel used in iso-butane combustion. Journal of Alloys and Compounds. 2010; 492:500–507.

[36] Wu X, Wei Z, Chen X, et al. Effects of Cobalt Doping on the Microstructure and Optical Properties of $ZnAl_2O_4$ Nanoparticles. Russian Journal of Physical Chemistry A. 2017; 91:2651–2656.

[37] Ianos R, Lazau R, Lazau I, et al. Chemical oxidation of residual carbon from $ZnAl_2O_4$ powders prepared by combustion synthesis. Journal of the European Ceramic Society. 2012; 32:1605–1611.

[38] D'Ippolito V, Andreozzi GB, Bosi F, et al. Crystallographic and spectroscopic characterization of a natural Zn-rich spinel approaching the end member gahnite ($ZnAl_2O_4$) composition. Mineralogical Magazine. 2013; 77:2941–2953.

[39] Chopelas A, Hofrmeister AM. Vibrational Spectroscopy of Aluminate Spinels at 1 atm and of $MgAl_2O_4$ to Over 200 kbar. Phys Chem Minerals. 1991; 18:279-293.

[40] Fang CM, Loong C-K., de Wijs GA, et al. Phonon spectrum of $ZnAl_2O_4$ spinel from inelastic neutron scattering and first-principles calculations. Physical Review B. 2002; 66.144301.

[41] Cynn H, Sharmaand SK, Cooney TF, et al. High-temperature Raman investigation of order-disorder behavior in the $MgA1_20_4$ spinel. Physical Review

B. 1992; 45:500-502.

[42] Motloung SV, Dejene FB, Swart HC, et al. Effects of Cr^{3+} mol % on the structure and optical properties of the $ZnAl_2O_4:Cr^{3+}$ nanocrystals synthesized using sol–gel process. Ceramics International.2015; 41:6776–6783.

[43] Motloung SV, Dejene FB, Koao LF,et al. Structural and optical studies of $ZnAl_2O_4$: x% Cu^{2+} (0< x ≤ 1,25) nanophosphors synthesized via citrate sol-gel route. Optical Materials.2017; 64:26-32.

[44] Motloung S.V, Tsega M, Dejene FB, et al. Effect of annealing temperature on structural and optical properties of $ZnAl_2O_4$:1.5% Pb^{2+} nanocrystals synthesized via sol-gel reaction. Journal of Alloys and Compounds. 2016; 677:72–79.

[45] Motloung SV, Dejene FB, Swart HC, et al. Effect of Zn/citric acid mole fraction on the structure and luminescence properties of the un-doped and 1.5% Pb^{+2} doped $ZnAl_2O_4$ powders synthesized by citrate sol-gel method. Journal of luminescence. 2015; 163 :8-16.

[46] Konan KF, Hartiti B, AKA B, et al. Thevenin, Propriétés structurales et optiques de couches minces d'oxyde de zinc (ZnO) texturées (002) par voie sol-gel via spin-coating. Afrique SCIENCE. 2010; 06:29 – 37.

[47] Tangcharoen T, T-Thienprasert J, Kongmark C. Optical properties and versatile photocatalytic degradation ability of MAl_2O_4 (M=Ni, Cu, Zn) aluminate spinel nanoparticles. Journal of Materials Science: Materials in Electronics. 2018;29:8995–9006.

[48] Pramauro E, Vincenti M, Augugliaro V, et al. Photocatalyticdegradation of Monuron in aqueoustitaniumdioxide dispersions. Environmental Science &Technology. 1993;27:1790–1795.

[49] Ollis DF, Pelizzetti E, Serpone N, Photolysis Fundamentals and Applications, eds. John. Wiley and sons (Toronto, Canada). Chapter. 1989;18:603-637.

[50] Elhalil A., Elmoubarki R., Sadiq M., et al. Enhanced photocatalytic degradation of caffeine as a model pharmaceutical pollutant by Ag-ZnO-Al_2O_3 nanocomposite. Desalination and Water Treatment. 2017;94:254–262.

[51] Kiran VS, Sumathi S. Dielectric studies on Bismuth substituted Zinc aluminate Nanoparticles. ChemTech. Research. 2015;8:097-103.

[52] Iqbal MJ, Farooq S. Effect of doping of divalent and trivalent metal ions on the

structural and electrical properties of magnesium aluminate. Mater. Sci. Eng., B. 2007;136:140-147.

[53] Iqbal MJ, Kishwar B. Electrical properties of $MgAl_{2-2x}Zr_xM_xO_4$ (M = Co, Ni and x = 0.00–0.20) synthesized by co precipitation technique using urea. Mater. Res. Bull. 2008; 44:753-758.

[54] Iqbal MJ, Ismail B, Electric, dielectric and magnetic characteristics of Cr^{3+}, Mn^{3+} and Fe^{3+} substituted $MgAl_2O_4$: Effect of pH and annealing temperature. J. Alloys Compd. 2009; 472:434-440.

[55] Iqbal MJ, Ismail B. Correlation between structural and electrical properties of $Mg_{1-2x}Zn_xNi_xAl_2O_4$ (x = 0.0–0.5) ceramic nanomaterials synthesized by a urea assisted microwave combustion method. J. Alloys Compd. 2010; 504:440-445.

Figures

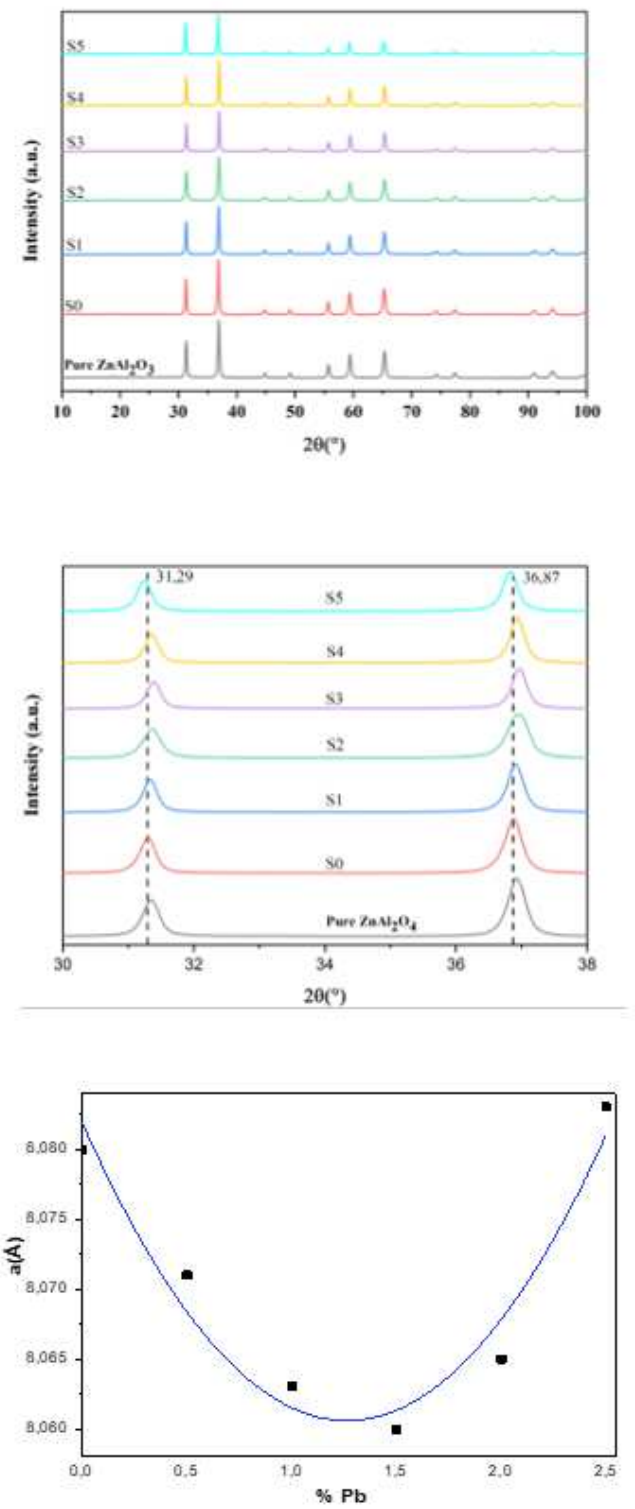

Figure 1

Fig. 1.a: XRD diagrams of pure ZnAl2O4 and samples S0, S1, S2, S3, S4 and S5. Fig.1.b: Shift of The most intense (220) and (311) diffraction peaks of pure ZnAl2O4 and Samples S0, S1, S2, S3, S4 and S5. Fig.1.c: The variation of the lattice parameter of the samples versus of the % Pb2+.

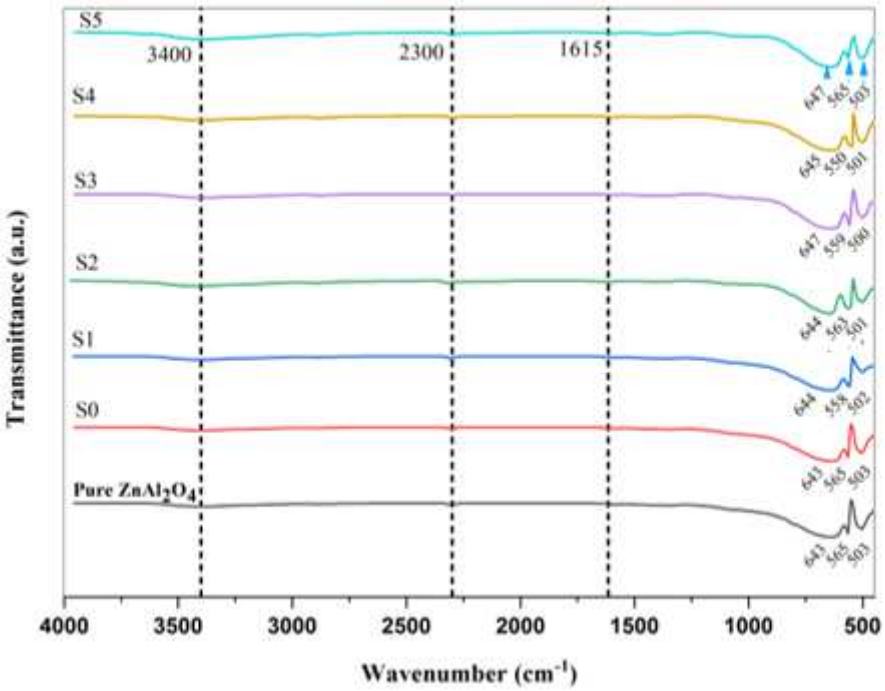

Figure 2

represents the IR spectra of the samples pure ZnAl2O4 and S0, S1, S2, S3, S4 and S5.

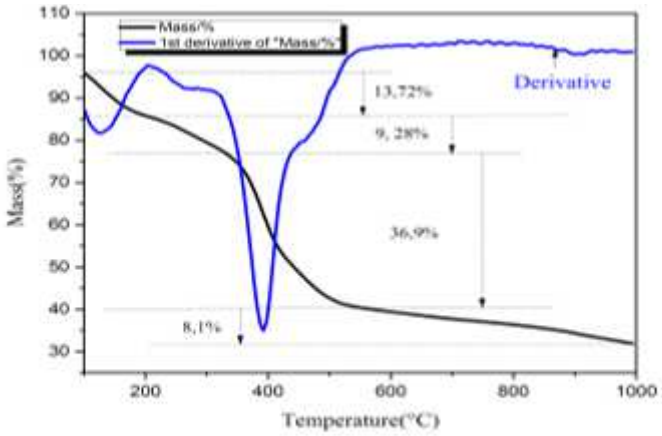

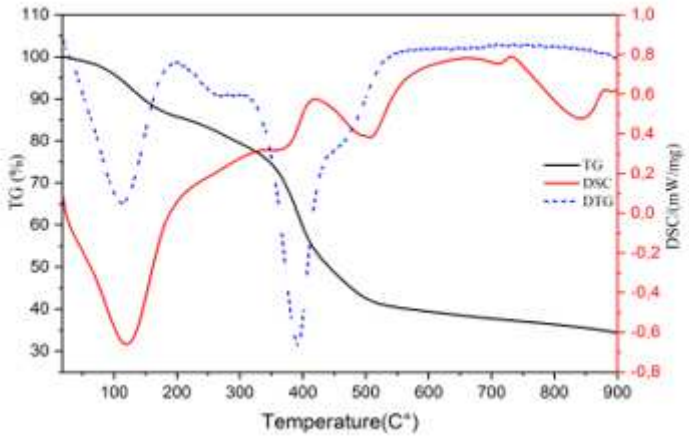

Figure 3

Fig.3.a: DTG of pure ZnAl2O4. Fig.3.b: DSC of pure ZnAl2O4.

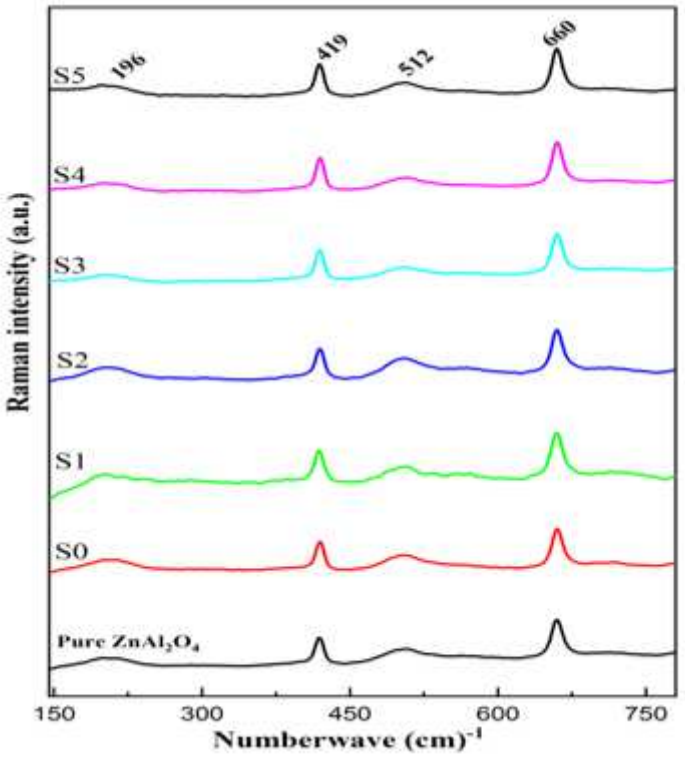

Figure 4

Raman spectra undoped and doped ZnAl2O4 annealed at 900°C

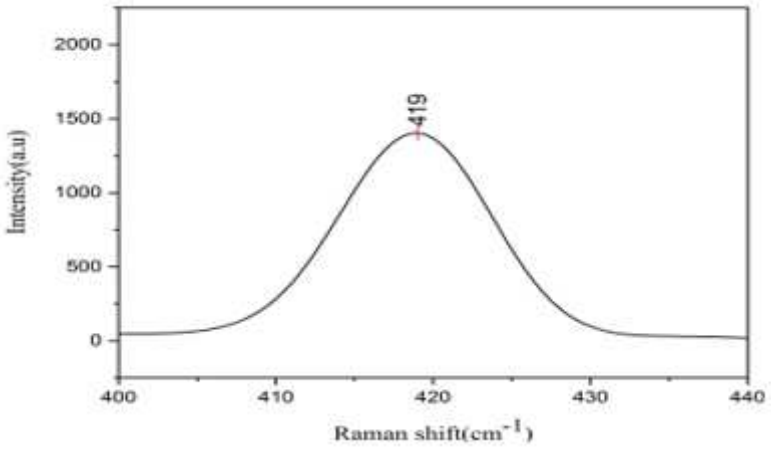

Figure 5

detail of the 419 cm-1 peak, symmetric Gaussian curve fitting, indicating a Negligible asymmetry

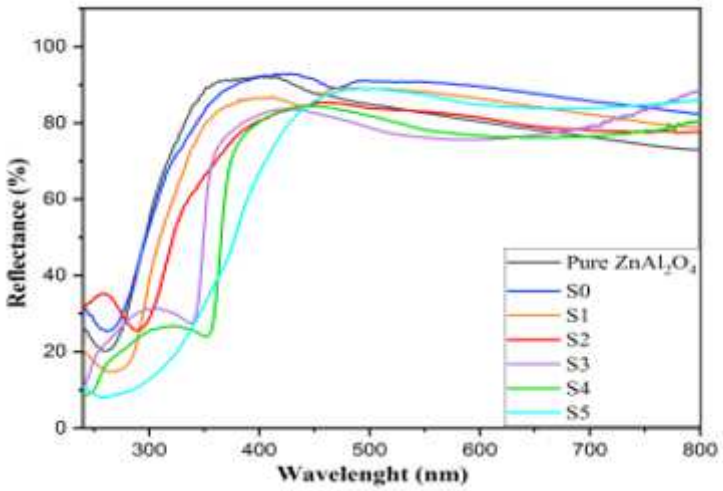

Figure 6

Reflectance of the samples pure ZnAl2O4 and S0, S1, S2, S3, S4 and S5

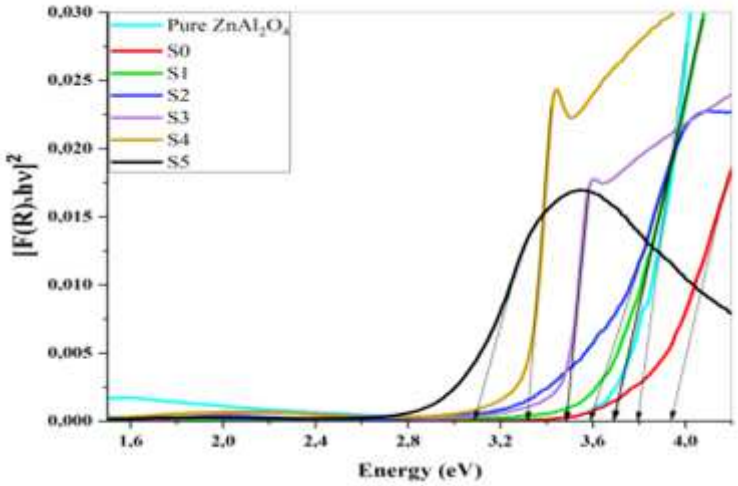

Figure 7

Eg determination

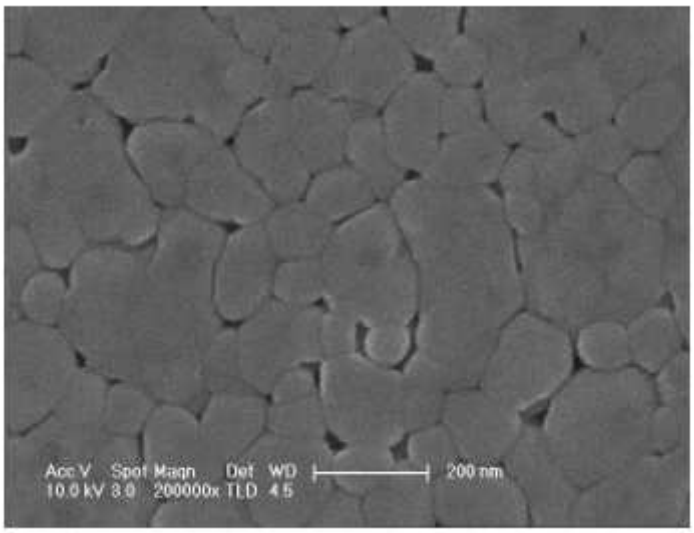

Figure 8

SEM micrographs of ZnAl2O4 nanoparticles synthesized

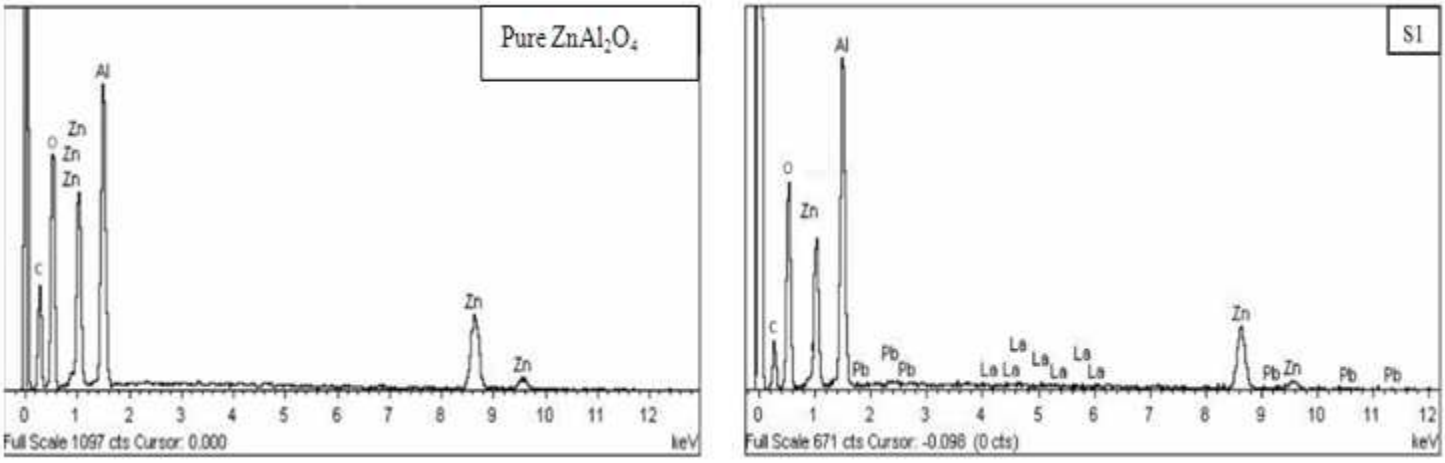

Figure 9

EDX spectra for: a) pure ZnAl2O4 and b) sample S1

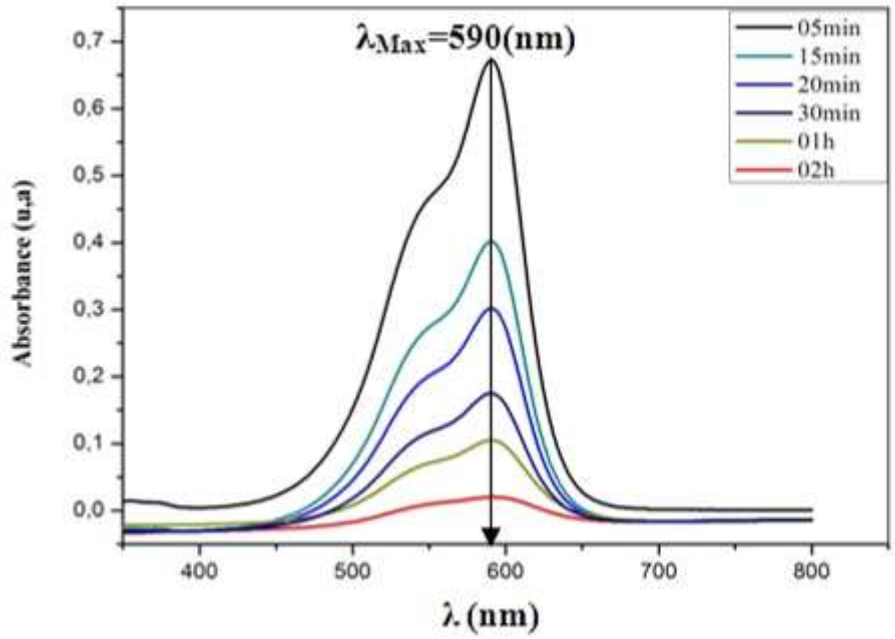

Figure 10

Absorbance of HCV in presence of ZnAl2O4

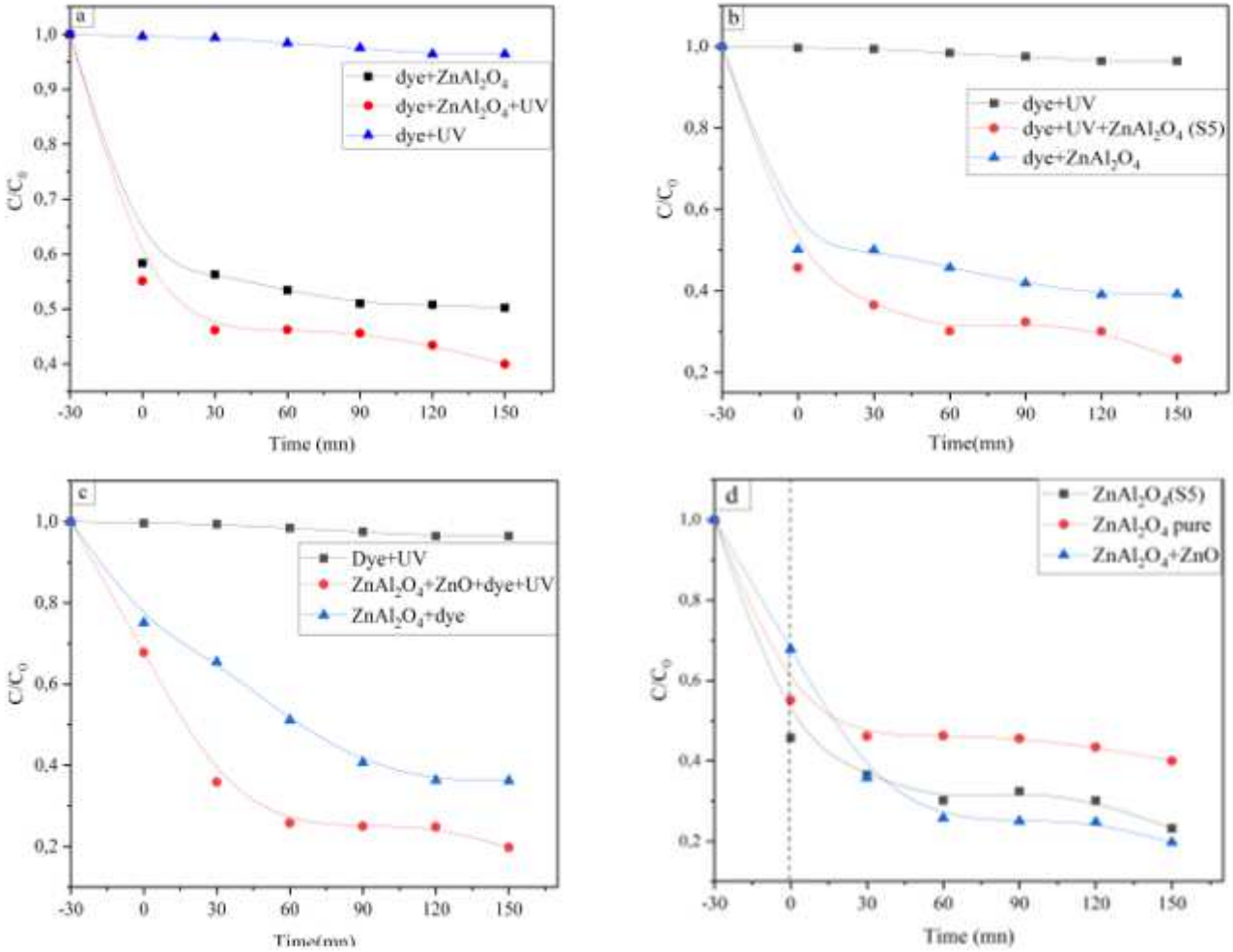

Figure 11

Photocatalytic activity of the ZnAl2O4 pure; ZnAl2O4 (S5) and ZnAl2O4+ZnO